ESA Contract No. 4000135209/21/NL/AR

241-ES.2458 Straylight Lidar OGSE Verification Tool

Executive Summary Report

Issue 1, Rev. 0

19.08.2024

ESA Contract No. 4000135209/21/NL/AR

	Name
Authors	Eleonoor Bosch (CSEM)
Project manager	Eleonoor Bosch (CSEM)
Contract officer	Fabien Droz (CSEM)

CSEM – Centre Suisse d'Électronique et de Microtechnique (CH)

Distribution List

Name	Organisation	Copies
Authors	CSEM	pdf
M. Simon Strottman	Central Registry Office EUROPEAN SPACE RESEARCH AND TECHNOLOGY CENTRE P.O. Box 299 2201 AG NOORDWIJK The Netherlands	pdf

Document Change Record

Issue	Rev.	Date	Modified pages and description/reason
1	0	**19.08.2024**	First version

REFERENCES

[1] V. Kirschner, "Stray Light Analysis and Minimization," in *ESA course on Space Optics Instrument Design & Technology*, 2017, p. 132.

[2] G. Peterson, "Stray light test station for measuring point source transmission and thermal background of visible and infrared sensors," in *Proc. SPIE*, 2008. doi: 10.1117/12.794898.

[3] Q. Chen, Z. Ma, X. Li, Z. Pang, L. Xu, and Z. Li, "Stray light measurement for point source transmittance of space optical systems," in *Proc. SPIE 9684*, 2016, p. 96842V. doi: 10.1117/12.2243405.

[4] L. Clermont, W. Uhring, M. Georges, W. Khaddour, P. Blain, and E. Mazy, "Advances in stray light characterization by ultrafast time-of-flight imaging," in *International Conference on Space Optics — ICSO 2022*, K. Minoglou, N. Karafolas, and B. Cugny, Eds., Dubrovnik, Croatia: SPIE, Jul. 2023, p. 33. doi: 10.1117/12.2689033.

[5] L. Clermont, P. Blain, W. Khaddour, and W. Uhring, "Unlocking stray light mysteries in the CoRot baffle with the time-of-flight method," *Sci. Rep.*, vol. 14, no. 1, p. 6171, Mar. 2024, doi: 10.1038/s41598-024-56310-z.

[6] A. Mora *et al.*, "Gaia: focus, straylight and basic angle," in *Proc. SPIE*, 2016, p. 99042D. doi: 10.1117/12.2230763.

[7] S. M. Pompeaa, R. N. Pfisterer', and J. S. Morganc, "A Stray Light Analysis of the Apache Point Observatory 3.5- Meter Telescope System".

[8] G. De Vine, B. Ware, K. McKenzie, R. E. Spero, W. M. Klipstein, and D. A. Shaddock, "Experimental Demonstration of Time-Delay Interferometry for the Laser Interferometer Space Antenna," *Phys. Rev. Lett.*, vol. 104, no. 21, May 2010.

[9] S. R. Sankar and J. C. Livas, "Optical telescope design for a space-based gravitational-wave mission," in *Proceedings SPIE 9143, Space Telescopes and Instrumentation 2014: Optical, Infrared, and Millimeter Wave*, Aug. 2014.

[10] J. C. Livas and S. R. Sankar, "Optical telescope system-level design considerations for a space-based gravitational wave mission," in *Proceedings Volume 9904, Space Telescopes and Instrumentation 2016: Optical, Infrared, and Millimeter Wave*, Edinburgh, United Kingdom, Jul. 2016.

[11] W. Brzozowski *et al.*, "The LISA optical bench: an overview and engineering challenges," in *Space Telescopes and Instrumentation 2022: Optical, Infrared, and Millimeter Wave*, L. E. Coyle, M. D. Perrin, and S. Matsuura, Eds., Montréal, Canada: SPIE, Aug. 2022, p. 22. doi: 10.1117/12.2627465.

[12] "Hybrid Photon Detector HPM-100-06," Becker & Hickl GmbH, May 2023. Accessed: Jul. 29, 2024. [Online]. Available: https://www.becker-hickl.com/wp-content/uploads/2023/05/db-hpm-06-07-v03.pdf

[13] W. Becker, V. Shcheslavskiy, and P. Morozov, "World Record in TCSPC Time Resolution: Combination of bh SPC-150NX with SCONTEL NbN Detector yields 17.8 ps FWHM," Becker & Hickl GmbH. Accessed: Jul. 29, 2024. [Online]. Available: https://www.becker-hickl.com/zh/literature/application-notes/world-record-in-tcspc-time-resolution-combination-of-bh-spc-150nx-with-scontel-nbn-detector-yields-17-8-ps-fwhm/

[14] "Single Quantum, SNSPDs: SQCam," Single Quantum. Accessed: Jul. 29, 2024. [Online]. Available: https://www.singlequantum.com/technology/cryogenics/

[15] "InSight®X3+™ and InSight®X3™ Tunable Ultrafast Lasers," Spectra-Physics. Accessed: Jul. 29, 2024. [Online]. Available: https://www.spectra-physics.com/en/f/insight-x3-tunable-laser

INTRODUCTION

Straylight contributions represent a major issue for astronomical observation instruments and can degrade the image quality substantially when not corrected for. It can affect the accuracy of radiometric measurements, reduce the contrast and the SNR of images or generate artificial objects.

Several mechanisms are responsible for causing straylight disturbances: rogue paths, ghosts, scattered light at optical or structural surfaces, and diffraction. Surface scattering or reflectance is generally defined by the bi-directional scatter/reflectance distribution function (BSDF or BRDF), which represents the ratio between the incident irradiance at a certain angle and the radiance of the surface in each direction.

In order to limit the effects of straylight, dedicated baffles and vanes need to be designed while considering the impact on the volume, mass and cost of a system, it is key to properly address the unintended light paths without over shielding the design [1].

To quantify the straylight performance of a system, the main figure of merit is the point source transmittance (PST) of the instrument. The PST represents a transfer function relating the irradiance at the focal plane due to straylight mechanisms to the irradiance at the entrance aperture in function of the angle of incidence, for a distant point source.

Straylight in a baffle can be simulated with optical ray tracing software such as GUERAP, APART, ASAP, TracePro or LightTools. The software used in SLOTT was ASAP which requires a model of the baffle and the test positions for the light source. It can then provide the expected signal amplitude and time of flight at the detector position which can be compared to the measurement results. The simulations take several hours, despite the recent advancements in the calculation speed of the software.

Some portable breadboard systems have been designed for the measurement of BSDF of certain materials and coatings, which provide information about the components but are not suitable to measure complete systems.

It is possible to obtain a full characterization of an instrument PST by the use of dedicated test stations, such as available at the Breault Research Organization [2]. Using a large collimator mounted on a gimbal, this facility allows measuring PST of instruments with apertures up to 30cm in a vacuum environment. More recently, another group reported on the assembly of a similar test station accommodating larger instruments up to 1 m aperture in a class 6 cleanroom for PST characterization at VIS and IR wavelengths [3].

The drawbacks of such facilities are the large bulk that occupies a full laboratory room and the limited dynamic range to 5-7 orders of magnitude.

Time-of-flight (TOF) measurements can be performed directly by measuring the time taken for a short light pulse to travel back and forth to a target (see Figure 1). With this, multiple echoes can be resolved from a single pulse.

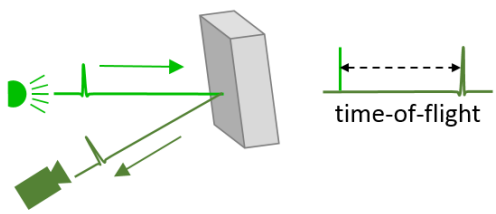

Figure 1: Principle of direct TOF measurement

Direct ToF systems use a highly sensitive sensor such as an APD (avalanche photodiode), a single-photon APD (SPAD) or a silicon photomultiplier (SiPM), which consists of an array of SPADs connected in parallel. These detectors provide a very high sensitivity, down to single-photon level, but with some inherent uncertainty in photon arrival time, called jitter.

A system based on direct TOF measurements with a SPAD-based detector presents the following advantages for straylight detection:

1. The ability to time-resolve straylight sources.
2. Sufficient sensitivity to characterize typical PST attenuation (10^{-13}).
3. An acquisition time of around a few hours at most for typical instruments.
4. Flexibility depending on the application requirements, allowing to optimize for sensitivity, focal plane resolution and bandwidth.

Additional validation and application of this approach has been demonstrated at the Centra Spatial de Liège (CSL) where another direct time of flight lidar system was used to analyze the CoRoT baffle [4], [5]. The researchers were successfully able to identify straylight sources such as dust inside the baffle, as well as separate sources intrinsic to the baffle from those contributed by the experimental setup. The spatial and temporal separation of the straylight signals significantly improved straylight identification, and enabled measurement outside of a vacuum chamber [5].

BREADBOARD DESIGN

The detailed design of the breadboard consists of an illumination module, a timing module, and a detector module. The Illumination module and detector module stand opposite one another on either side of the test baffle, as shown in Figure 2.

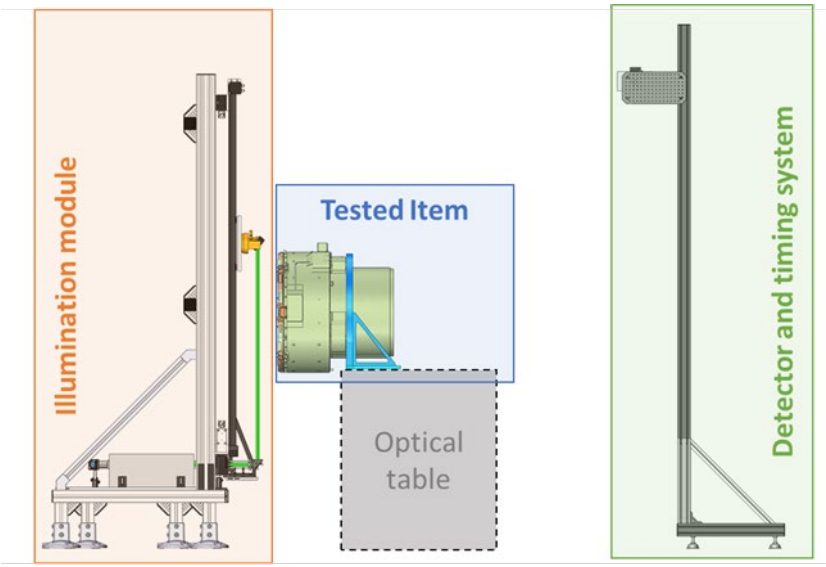

Figure 2: SLOTT Breadboard Overall Design Drawing

The illumination module, shown in detail in Figure 3, is capable of scanning around the aperture of a baffle up to 1m in diameter with 5cm spatial resolution. The gimbal angle is adjusted manually. The scan positions are automated, and the optical path length is recalculated at each position in software. The

beam path includes a beam expander which can have variable expansion depending on the lenses selected. There is additional room in the beam path for optical filters or other components.

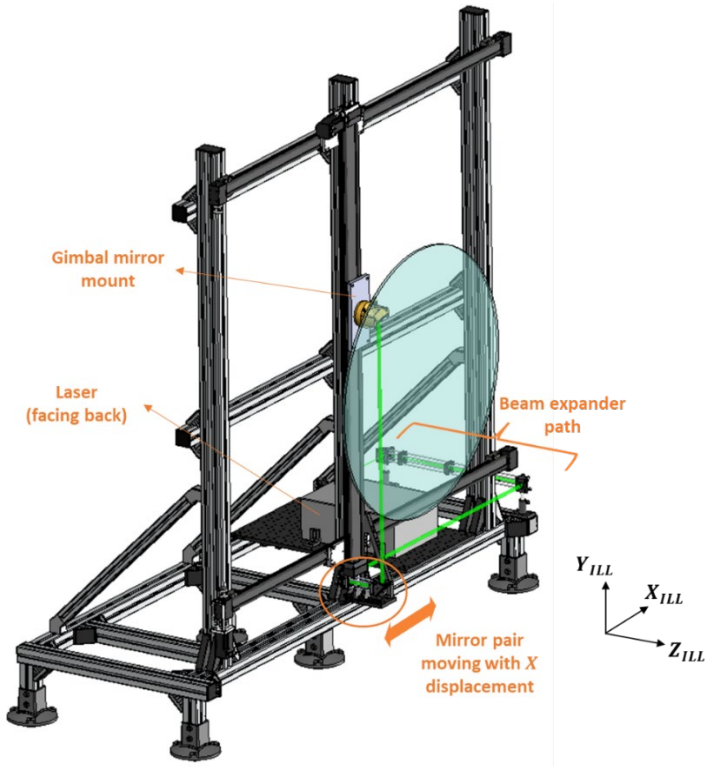

Figure 3: Illumination module CAD with telescope aperture representation

Several photon detector types were considered, but SPADs were ultimately preferred over Photomultiplier Tubes (PMTs), superconducting single-photon detectors, and Hybrid detectors. PMTs were determined to have too low timing performance compared with the other technologies. And superconducting single photon detectors are complex to handle, bulky, and require liquid helium cooling – they were determined too complex and expensive for this project.

The Becker and Hickl HPM-100 hybrid detector was selected with active area (3mm), low dark count rate (50cps) and high timing resolution (impulse response of 18ps at FWHM). The detector sensitivity to visible light, which outperforms detectors which are sensitive to infrared light, was one of the driving factors in laser selection.

A Prospective Instruments FSX-520 laser at 520nm with a repetition rate of 40MHz was selected to optimize the system ambiguity range (which needed to be greater than 6m) and pulse energy at a wavelength compatible with the detector.

A summary of the main design choices and system parameters is provided in Table 1.

Table 1: OGSE Main Parameters

Parameters	Value	Comment
Laser parameters		
Wavelength	520 nm	
Laser average power	3 W	

Repetition rate	40 MHz	
Laser pulse energy	75 nJ	
Illumination beam diameter	Adaptable: 2, 6.7, 10, 16.7 and 26.6 mm	
Detection and timing system parameters		
Expected time resolution	< 20 ps	This corresponds to ~ 6 mm
Quantum efficiency (@520 nm)	10 %	
Active area	Ø 3 mm (7.06 mm^2)	
Dark count	50 cps	
Scanning mechanism parameters		
X-axis translation range (horizontal)	1 500 mm	
Y-axis translation range (vertical)	1 250 mm	
Translation repeatability (X and Y)	0.5 mm	
Θx-axis gimbal range	0° to -65°	Limited by measurement setup configuration.
Θy-axis gimbal range	-65° to +65°	

The timing module was implemented with reverse start-stop which was chosen because the inter-pulse time at a laser repetition rate in the tens of MHz is much shorter than the recovery time of the detector and timing module. The timer is started when a photon is detected and stopped a signal created by delaying the laser sync signal which follows each pulse. The delay is always set to be larger than the optical path length given the current gimbal position. The start stop implementation is depicted in Figure 4.

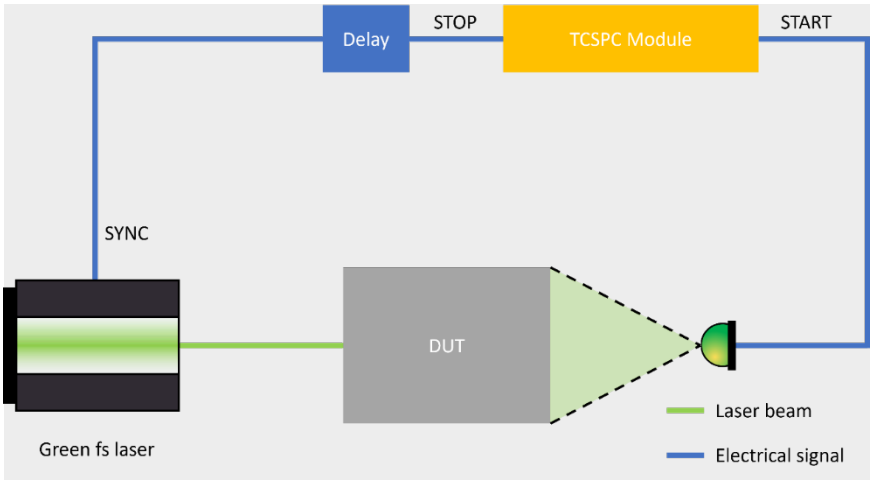

Figure 4: Summary of reverse start-stop timing implementation

Four TCSPC modules were considered for the breadboard, and of these the module with the highest timing resolution and best timing performance was chosen: the Becker & Hickl SPC-130INXX with 1.1ps timing performance and 203fs bin width. This module is also fully compatible with the selected detector.

A full block diagram of the system electronics is shown in Figure 5.

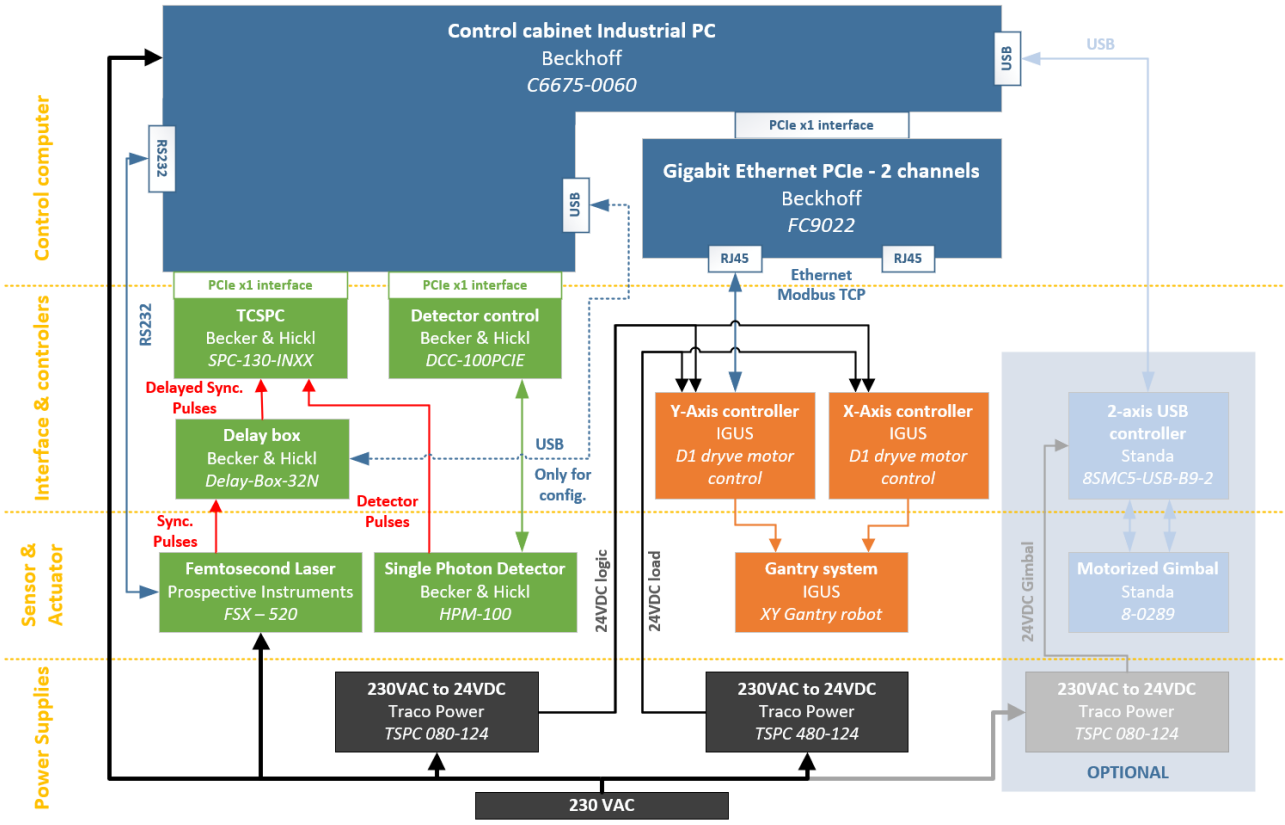

Figure 5: Control electronic architecture

SYSTEM PERFORMANCE

The system depth resolution achieved was 10mm – meaning that straylight sourced which have as low as a 10mm difference in optical path length can be distinguished by the system. This was verified both by measuring the impulse response of signal seen at the detector, and by reflecting the laser off two objects 10mm apart back at the detector. The results of the test are shown in Figure 6.

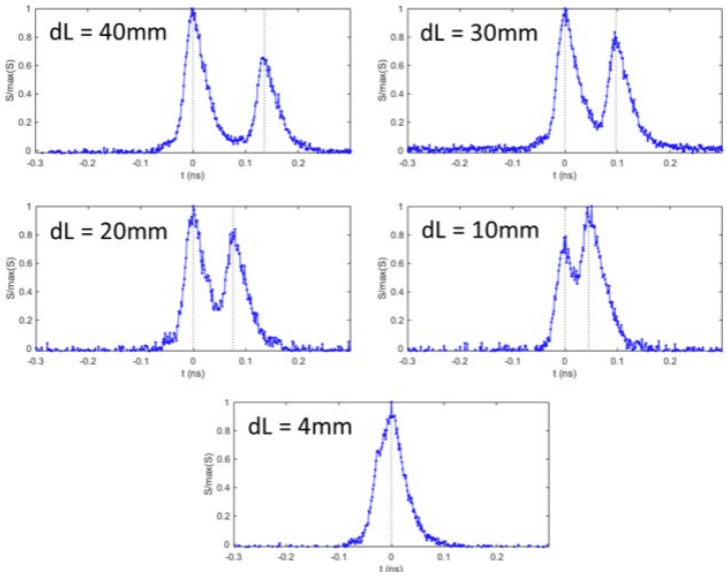

Figure 6: Depth resolution test results

The demonstrated system dynamic range was 10^0 to $1.3x10^{-13}$, when using the maximum possible laser power of 7A, as shown on the lowest line in Figure 7.

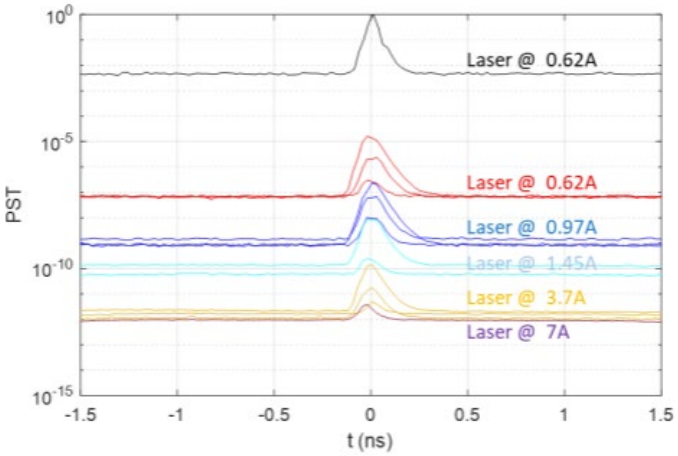

Figure 7: Dynamic range test results

Based on the maximum expected path length for straylight scattered inside the baffle (about 1.1m) and the measurements of 10ns length (2.99m) the data included light scattered or emitted from objects outside the baffle. Possible candidates for these noise sources are the beam expander or the lens barrels. Further possible sources of lower flux noise with shorter path length than baffle-scattered light are the lens surfaces, mirrors, and other illumination module components.

All baffle vanes and two of the walls were tested. Vane 1, Wall 0-1, Wall 1-2, Vane 3, Vane 5 and Vane 7 had a very good match with simulation results.

Vane 2, Vane 4 and Vane 6 had measurement data differed somewhat in the expected time of flight or flux level of the peaks measured in the signal.

Examples of Vane 1 and Vane 2 measurements compared with their simulation results are shown in Figure 8 and Figure 9.

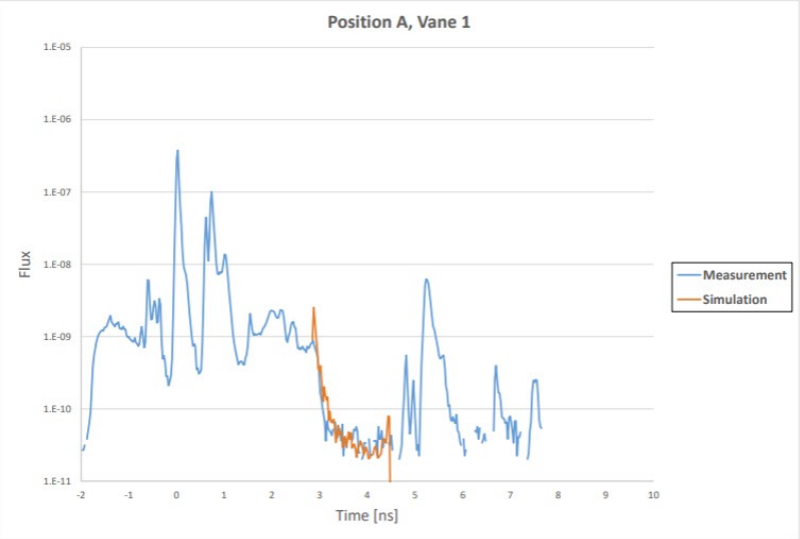

Figure 8: Vane 1 measurement and simulation overlay

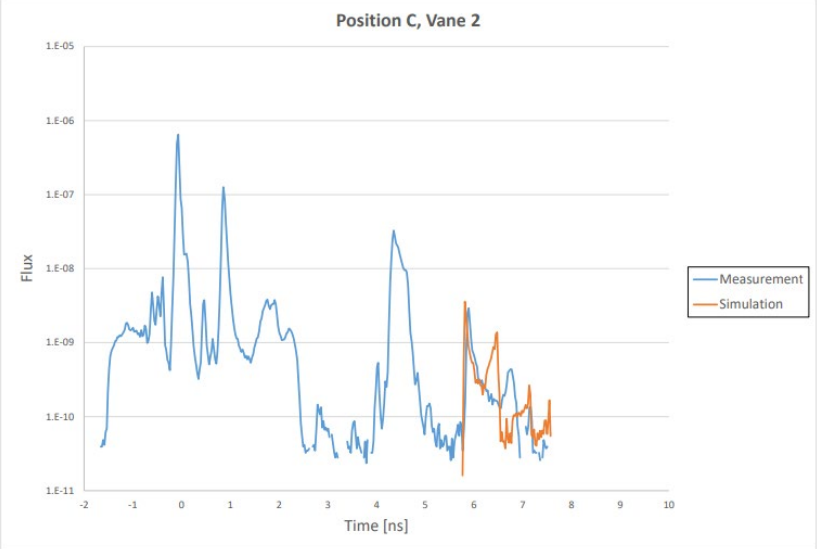

Figure 9: Vane 2 measurement and simulation overlay

DISCUSSION AND OUTLOOK

The OGSE as-built already demonstrates performance which is sufficient to conduct time-resolved stray light measurements. It has a high dynamic range, as required for the CHEOPS baffle, which was measured. And the depth resolution to 10mm was more than sufficient for these tests. Several improvements can still be made to enable use with a wide variety of telescopes.

By replacing the 1'' gimbal mirror with a 2'' mirror the beam should be prevented from being vignetted at large elevation angles, when measurements require extreme entrance angles to the aperture. Additionally, particular care can be taken to improve the isolation of the DUT from external light sources and reflective surfaces to reduce contributions from outside of the DUT.

The hybrid photon detector HPM-100-06 from Becker and Hickl has a spectral range of 220 to 650 nm [14]. Currently, no conventional single-photon detector covers the entire spectrum range of 400 nm to 1700 nm with the required timing performance. However, superconducting single-photon detectors (SSPDs) have demonstrated impulse response functions of 17.8ps FWHM and offer a broad spectral range from 0.5 µm to 2.5 µm, which largely covers the range required by most telescopes [15]. Additionally, they provide a high quantum efficiency (> 85%) and a faster count rate than conventional detectors. These detectors are typically fiber-coupled, but free-space compatible versions are also available.

SSPDs require laboratory infrastructure for liquid helium cooling. The system automatically manages the cooling and helium recovery process. This is the only technology to date offering timing performance of <30ps across a large spectral range, including, for example, the working wavelength of the LISA telescope (1064 nm). For the BB, SSPDs were out of scope but should be carefully reconsidered for future developments if the lab infrastructure can support them.

One software limitation of the BB is the maximum count rate per bin. The software currently limits this to 2^{16}, but switching the collection mode would make it unlimited, further increasing the depth resolution.

For further dynamic range, a tuneable femtosecond laser could offer several watts of optical power in the spectral range of 680 nm to 1300 nm. However, such lasers cost around 200kEuro and are relatively large (around 1 meter in length).

Finally, the OGSE may be tested and then adapted for cleanliness and use in an optical clean room environment.

CONCLUSION

During the SLOTT project, a time-of-flight OGSE straylight measurement breadboard was designed and built for testing with a representative telescope baffle. The breadboard design was for a baffle of maximum 1m diameter and was built to be transportable and with automated measurement capability. The system performed well when tested with the CHEOPS baffle model in several test positions. The time-of-flight results were compared with simulations and showed a good match for the measured straylight in each position. Some sources of noise were identified in the measurements which could be addressed in a future iteration of the straylight OGSE.

The working TRL 4 system demonstrates the utility of using time-of-flight for straylight analysis and the opportunity to significantly reduce the lab space required and to speed up measurement time. Time-of-flight straylight detection systems can also be built to be compatible with cleanroom environments.

The SLOTT OGSE competes with streak-camera time-of-flight systems which offer greater resolution, as such the SLOTT setup may be most interesting if adapted for longer wavelengths which are not compatible with streak camera detectors on the market.

The SLOTT project enabled validation of time-of-flight straylight detection scheme using a green laser and single pixel SPAD with high timing performance for distinguishing straylight sources. The breadboard system has demonstrated a temporal resolution below 30ps, equating to a spatial resolution of less than 9 mm and a dynamic range of 10^{-13}, successfully meeting the requirements outlined for the system performance and exceeding the state of the art.